Applied Materials Today 19 (2020) 100571

Contents lists available at ScienceDirect

Applied Materials Today

journal homepage: www.elsevier.com/locate/apmt

Raman scattering obtained from laser excitation of $MAPbI_3$ single crystal

Tal Ben-Uliel[a,1], Hagit Aviv[a,1], Junjie Zhou[b,1], Minghao Li[b], Shalom Avadyayev[a], Omree Kapon[a], Vinayaka Damle[a], Chenyi Yi[b,*], Yaakov Tischler[a,*]

[a] Department of Chemistry and Bar Ilan Institute for Nanotechnology and Advanced Materials, Bar Ilan University, Ramat Gan, 5290002, Israel
[b] State Key Laboratory of Power System, Department of Electrical Engineering, Tsinghua University, Beijing, 100084, China

ARTICLE INFO

Article history:
Received 14 August 2019
Received in revised form 14 January 2020
Accepted 17 January 2020

Keywords:
Methylammonium lead iodide
Single crystal
Phase transition
Low frequency Raman
Stimulated Raman

ABSTRACT

Finding renewable energy sources is of paramount importance to meet the increasing global energy demand whilst minimizing the impact on the environment. The research community has focused on solar energy as it is endlessly available, and have ranked the methylammonium lead iodide ($MAPbI_3$) as one of the most promising candidate amongst perovskite solar cells. Despite its high efficiency, the $MAPbI_3$ is sensitive to humidity, light, and temperature, its instability affects primarily on the crystalline structure and eventually leads to degradation. Three crystalline structures are known for this material, orthorhombic, tetragonal, and cubic which exist in different temperatures. Here we report on several processes detected from laser excitation of $MAPbI_3$ single crystal at ambient conditions. A phase transition from tetragonal to cubic phase was induced by excitation of over 15 mW laser power. The phases were characterized by LF-Raman and photoluminescence, taken simultaneously with the increase of exciting laser power and the spectral changes were assigned to the structural differences. In addition, Raman stimulation of iodine vapors signal was observed, those vapors were generated from the core of the focus wherein the highest temperature led to degradation. The stimulated Raman phenomenon was enabled due to the unique properties of the $MAPbI_3$ single crystal and revealed viability to use this material for additional applications in other research fields.

1. Introduction

Tremendous efforts are made worldwide in the search for renewable energy sources due to increasing global demand for energy, reduction in fuel-based energy sources, and environmental responsibility concerns. The most promising renewable energy source is the solar energy, as it can be converted into electrical energy and is endlessly available. [1–3] Commercial solar cells are based mainly on silicon and other semiconductors and have established efficiencies that meet global energy demand. However, the high costs of the existing technologies lead to expanded search for cheaper alternative photovoltaic devices such as perovskite solar cells (PSCs) [4]. The promising performance of PSCs has been attributed to extraordinary material's properties, such as high absorption coefficient, [5] tunable bandgap [6], low exciton binding energy [7], and long charge carrier diffusion length [8]. The most widely used PSC material is methylammonium lead iodide ($MAPbI_3$), where MA is an organic cation at the center of a lead iodide cage structure. $MAPbI_3$ is sensitive to humidity, light, and temperature, its instability affects primarily on the crystalline structure and eventually leads to degradation. [2] Currently, the instability prevents from $MAPbI_3$ to achieve the market's requirements as a material for solar cell, hence extensive research has recently focused on the study of degradation mechanisms to improve the device stability. [2,9,10] Investigations on the structural characterization of $MAPbI_3$ have identified three polymorphs: orthorhombic, tetragonal, and cubic. An orthorhombic to tetragonal phase transition occurs around 165 K and a second transition from tetragonal to cubic phase occurs around 330 K. [11,12]

The different crystalline structures were characterized by X-ray diffraction (XRD), [13] neutron powder diffraction (NPD) [14], photoluminescence (PL) [15,16], and low frequency (LF) vibrations by THz absorption or LF-Raman. The assignment of the LF vibrations to the vibrational modes was suggested using several calculation methods [11,17,18].

Resonance Raman Scattering (RRS) occurs when the exciting beam is within the electronic absorption region and results a higher intensity of fundamental spontaneous Raman bands and in many cases lead to appearance of overtone bands. [19–21] Stimulated

* Corresponding authors.
E-mail addresses: yicy@tsinghua.edu.cn (C. Yi), yrt@biu.ac.il (Y. Tischler).
[1] Equally contributing authors.

https://doi.org/10.1016/j.apmt.2020.100571
2352-9407/

Raman Scattering (SRS) is a third-order nonlinear process that exhibits narrow-line emission from existing Raman shifts, this is normally generated using two synchronized pulsed lasers as single-frequency excitation sources, or a narrowband source synchronized with a broadband source for multiplex excitation [22]. For some materials under certain conditions, a high enough laser power may induce SRS using only one laser, even when the exciting laser is continuous wave (CW). This self-stimulated phenomenon is generally referred to as impulsive stimulated Raman scattering [23] or cascaded Raman process [24]. Self SRS was extensively investigated for ionic single crystals, it has been concluded that two main parameters influence the Raman gain, bigger crystal and larger ionic radius of the cation will be beneficial [25–28].

In this paper, we report on several processes obtained from laser excitation of $MAPbI_3$ single crystal. The main volume of the focus underwent a laser induced phase transition from tetragonal to cubic crystalline structure. The polymorphs were identified by PL and LF-Raman spectra as the PL indicates on the materials' bandgap and the LF-Raman provides information on low energy vibrations that are resulted by the spatial structure. Moreover, we report on a SRS process obtained from the cavity that is generated by the laser excitation at the core of the focus.

2. Experimental section

2.1. Materials

The following materials were purchased from MERCK: methylamine solution (CH_3NH_2, 33 wt % in absolute ethanol), hydroiodic acid (HI, 57 wt % in water, 99.99 %), Methylammonium iodide (MAI, 98 %), diethyl ether (99.7 %), PbI_2 (99.99 %), N,N-dimethylformamide (DMF, 99.8 %), gamma-butyrolacetone (99 %), 2-propanol (anhydrous, 99.5 %). Double distilled water was used, obtained by purifying water through a Barnstead EASY Pure II osmosis system (Thermo Fisher Scientific Inc.).

2.2. Synthesis of $MAPbI_3$ single crystal

$MAPbI_3$ single crystal was prepared by inverse temperature crystallization. Firstly, a mixture of 1:1 MAI and PbI_2 was dissolved in gamma-butyrolacetone to prepare 1.0 M $MAPbI_3$ solution at room temperature. Seed crystals were produced by heating the solution at 110 °C for 1 h. After that, a few seed crystals were selected to grow larger single crystals. An image of a typical tetragonal MAPbI3 single crystal is presented in Figure S1.

2.3. Synthesis of $MAPbI_3$ thin film

MAI was synthesized by reacting methylamine solution with hydroiodic acid under a nitrogen atmosphere at 0 °C for 2 h. The solvents were evaporated by a rotary evaporator providing a white-colored powder. The precipitate was washed several times with diethyl ether and dried under vacuum at 60 °C for overnight. The $MAPbI_3$ thin film was synthesized inside a glovebox (nitrogen atmosphere) using a two steps method, hence including two solutions. The first solution contained 1 M of PbI_2 stirred in DMF for overnight at 80 °C, and the second solution contained 0.2 M of MAI dissolved in 2-propanol right before the synthesis at 60 °C. The solutions were filtered prior to use by a PTFE filter with a pore diameter of 0.45 μm. The substrates used for the deposition were 25 × 25 mm of clean glass activated by oxygen plasma. First, a film of PbI_2 was fabricated on top of the substrate by spin coating 100 μL of PbI_2 solution at 4000 rpm for 60 s, followed by annealing at 100 °C for 60 min. Next, the PbI_2 film was dipped in the MAI solution for 5 min. A dark-brown color appeared, indicating the formation of the $MAPbI_3$ perovskite. The formed film with a thickness of 500 nm was washed with 2-propanol and annealed at 100 °C for 65 min.

2.4. Structure illustrations

Structural illustrations of the $MAPbI_3$ single crystal and distance calculations were performed by the Mercury program using CIF codes 291372 for the tetragonal phase and 250735 for the cubic phase from the Inorganic Crystal Structure Database ICSD.

2.5. Raman measurements

In general, for measurements of both LF-Raman spectral region and above, acquisition time and laser power varied between the measurements. For all measurements: exciting laser was CW, objective magnification was 100X, and groove density of the selected grating was 1800 g/mm. At least 20 different spots from multiple crystal faces in each crystal and at least 3 crystals were measured. Systems details: for the LF-Raman spectral region, an integrated laser with three VHG filters system (ONDAX, XLF-MICRO 532 nm) was used. The excitation wavelength was generated from a solid state, double frequency 532 nm (Nd:YAG laser). The laser output was routed to the sample through a microscope, and the Raman signal was fiber-coupled into an imaging spectrometer (Princeton Instruments, SP-2500i) with an EM-CCD camera (Princeton Instruments, Pro-EM 1600^2). For measurements of the spectral region of above the LF vibrations (above 200 cm^{-1}), three Raman systems were used. The first was described previously in this section (ONDAX). The second is micro-Raman instrument (HORIBA Scientific LabRAM HR), in which two wavelengths are available for excitation, 532 (Nd:YAG laser) and 784 nm (diode laser), the signal was collected to an integrated spectrometer through an open space. The third system is a multichannel Renishaw In Via Reflex spectrometer (Renishaw plc, Wotton-under-Edge, UK) coupled with a CCD detector (Peltier cooled). The excitation wavelengths were 514.5 (Ar-ion gas laser) and 380 nm (diode laser), here also the signal was collected to an integrated spectrometer through an open space.

2.6. PL measurements

The PL was taken with the micro-Raman instrument (HORIBA Scientific LabRAM HR) using exciting wavelength of 532 nm. At least 5 different spots from multiple crystal faces were measured in each crystal, at least 3 crystals were measured.

3. Results and discussion

Few crystalline structures were observed for $MAPbI_3$, orthorhombic is the existing phase below ≈165 K, tetragonal is stable in the range of 165−330 K, and in higher temperatures, cubic is the stable phase. We have focused on the phase transition that occurs around 330 K from tetragonal to cubic as illustrated in Fig. 1a and b, respectively. Calculations derived from XRD measurements have demonstrated a bigger Pb-I cage for the cubic phase as was also reported in literature. [29] The measured distances from the partial negative charge of the iodine atoms to the ammonium are 4 and 4.5 Å in the cubic phase unit cell and 3.6, 3.8, 4.1, and 4.9 Å in the tetragonal phase unit cell (measured from the cifs). This is expected to result a less restricted vibration of the MA within the Pb-I cubic cage.

We report on phase transition of a $MAPbI_3$ single crystal from tetragonal to cubic phase induced by a laser excitation at ambient conditions as presented in Fig. 2. The laser excitation was used both to determine the existing phase and, over a certain power, to heat the crystal enough to induce the phase transition. The phase

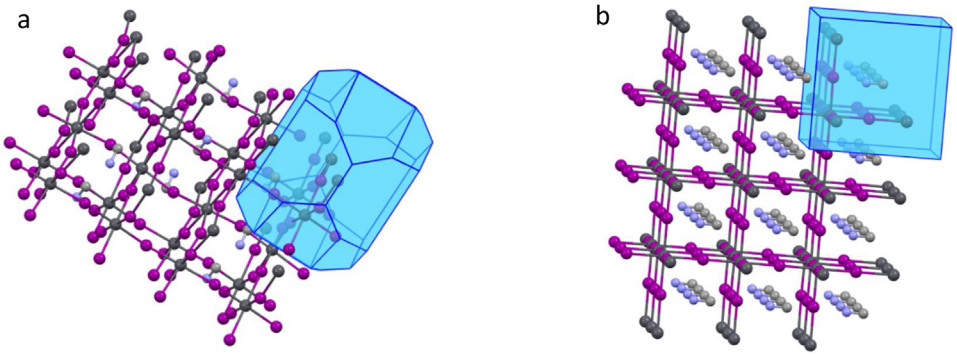

Fig. 1. Crystallographic image of the (a) tetragonal and (b) cubic $MAPbI_3$ structures.

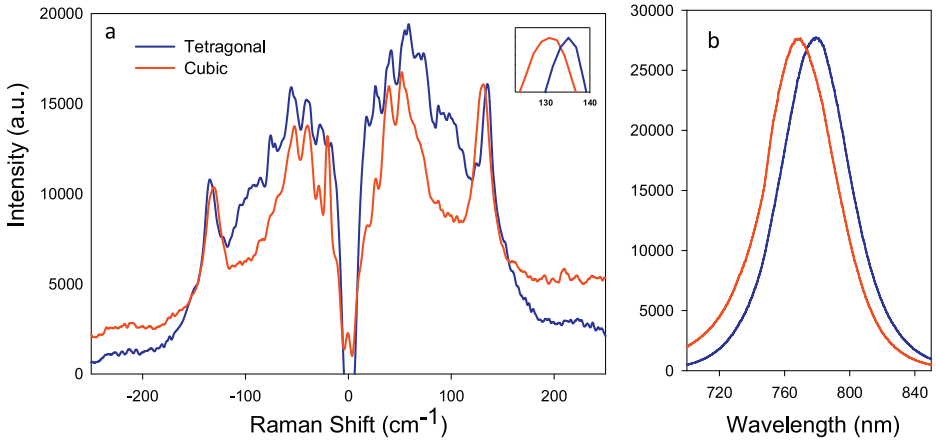

Fig. 2. (a) LF-Raman spectra and (b) PL of the tetragonal and cubic phase of $MAPbI_3$ before and after phase transition, respectively.

was identified by LF-Raman (Fig. 2a) and PL (Fig. 2b) measurements. At a low laser power, the tetragonal phase was detected, and over 15 mW, after 2 min of excitation and structural stabilization, the cubic phase was observed. Calculation confirmation for the conversion of energy to heat is complicated to achieve since it depends on many parameters, but in the case of exciting $MAPbI_3$ with 532 nm CW laser, we found evidence of the phase transition only above 15 mW. Theoretical calculations have assigned the vibrational modes in the spectral range of 20-60 cm^{-1} to the various vibrations of Pb-I-Pb. [18] The experimental Raman spectra demonstrate more active vibrational modes in this region for the tetragonal phase (blue curve) than the cubic phase (red curve), this can be explained by the lower symmetry of the tetragonal structure resulted by varied distances between the atoms of the inorganic cage. The spectral range of 60–100 cm^{-1} is assigned mainly to the lurching vibrational modes of the MA. The Raman shift at 135 cm^{-1} of the tetragonal phase is assigned to the MA liberation in the Pb-I cage; [17,18] this mode is blue shifted to 132 cm^{-1} in the cubic phase (magnification window in Fig. 2a) indicating a less restricted vibration, as expected from the previously mentioned distances between the positive charge and the partial negative charges. The PL spectra (Fig. 2b) correlate to the discussed phases according to literature, [15,16] hence support the existence of phase transition process. The spectrum of the cubic phase (red curve) demonstrates a blue shifting PL of the perovskite from 780 nm of the tetragonal to 770 nm indicating a wider bandgap, i.e. a higher energy gap with increasing temperature. Generally, for semiconductors (such as Si, Ge, and GaAs) the bandgap red-shifts to lower energies with increasing temperature. However, some Pb-based compounds show the opposite trend (such as PbS and $MAPbI_3$). [30] The bonding and antibonding splitting width depends on the overlap of

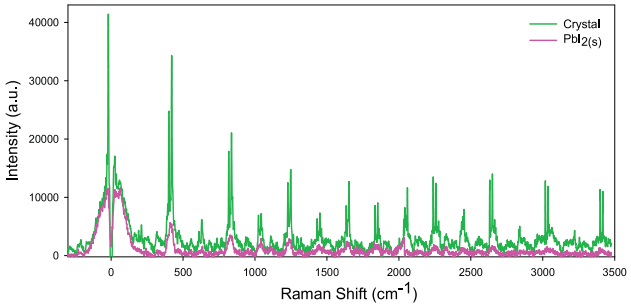

Fig. 3. SRS from the resonant vibrational mode when laser power crosses 15 mW (green plot), and RRS obtained from high laser power excitation of $PbI_{2(s)}$ (pink plot).

atomic orbitals and bonding strength. Therefore, increasing temperature that leads to lattice thermal expansion will impact both the valence band maximum and conductive band minimum levels. If both shift to the same direction, then the quantity of shift in the energy levels can be much larger than the change in the bandgap. For the temperature-dependent bandgap of $MAPbI_3$, it has been established that the bandgap increases with temperature. [15]

A couple of decomposition pathways have been suggested for $MAPbI_3$, [9,10,31] all involve the generation of $PbI_{2(s)}$ which can undergo further degradation to form $I_{2(g)}$ [32]. During high laser power excitation, the focused laser along with the material's sensitivity, generated decomposition at the core of the focus while the main focal volume underwent phase transition. As a result, iodine vapors were trapped inside a cavity within the $MAPbI_3$ single crystal. Fig. 3 presents a periodic narrow-lines emission from the measured spot of the single crystal (green plot). The laser energy

along a focal volume follows a Gaussian shape, hence the measured spot has a temperature gradient and the laser power required for phase transition in the majority of the focal volume, leads to a minimal decomposition at the core of the focus. Back in the 1970th, the Raman of iodine gas has been extensively investigated establishing RRS of the fundamental spontaneous Raman band at 213 cm^{-1} [21,33,34]. The condition for obtaining RRS is to excite the gas within its absorption region, therefore, the RRS can be achieved using quite a wide range of excitation wavelengths, such as 532 and 514.5 nm according to previously published $I_{2(g)}$ absorption spectrum. [35] We detected the reported resonant Raman by using 532 and 514.5 nm excitation but not by using 380 and 784 nm excitation wavelengths, as expected from the iodine absorption spectrum. A comparison between the RRS achieved from the single crystal (green plot) to that achieved from the excitation of PbI_2 powder (pink plot) indicates a clear non-linear process of narrow-lines emission from the RRS shifts of the single crystal. The non-linearity was analyzed by the peak intensity dependence in the laser excitation power, as presented in Figure S2. This process matches SRS and may be explained by one of the unique materials properties of $MAPbI_3$ single crystal such as non-linearity and ionic crystal. Nonlinear material is a precondition for the generation of SRS as it being a non-linear optical process [36,37] and ions within a crystal are known to affect the Raman signal gain as a factor of their radius [28]. The produced cavity has an important role in enabling the Raman stimulation since the cavity traps the iodine vapors where the walls are composed of ionic single crystal. This effect was not observed when we measured a spin coated $MAPbI_3$ film which can be attributed to the following causes, the generated cavity was too shallow to trap iodine vapors long enough for detection, and the structural continuity length was not sufficient for Raman stimulation. Longer single crystals were reported to exhibit better SRS due to higher light absorption. [25] The SRS spectrum shadows any other signal obtained from the measured spot for about 2 min, and as the iodine slowly diffuses out of the cavity, the LF-Raman of the cubic phase is revealed. Decreasing the laser power to $\leq$ 10 mW allows the crystal to cool back to room temperature and the exhibited Raman spectrum fits tetragonal phase. This shows that the phase transition is a reversible process. It is however important to emphasize that the decomposed part of the crystal is lost and excitation using high laser power for over 30 min is likely to decompose all of the focal volume. After a month of crystal's storage in ambient conditions, we could detect only the RRS without the SRS phenomenon, which we attributed to the adsorbed humidity that have changed the material's properties, for example by solvating the ions [38,39].

It is notable that the spontaneous Raman shift of the iodine at 213 cm^{-1} can be barely observed in Fig. 3, neither for the single crystal nor for the $PbI_{2(s)}$. This is explained by the collection of the scattered photons to the spectrometer in the LF-Raman system that is performed by an optical fiber rather than open space. Different fiber positioning affects the peaks intensity ratio and as a result can even hide signals [24]. Measuring the single crystal with high laser power using other systems have detected the spontaneous Raman shift of the iodine at 213 cm^{-1}. Fig. 4 presents the spectra taken with 532 nm (dark green plot) and 514.5 nm (brown plot) excitation wavelengths, both Raman systems are built to collect through open space, hence detecting the spontaneous shift. In addition, the narrow-line emission is clearly split to two lines using 532 nm, a solid state laser, while it appears as one line when 514.5 nm, a gas laser, is used for excitation. In general, a solid state laser outputs slightly broader emission than a gas laser, leading to slightly broader Raman shifts. Therefore, a possible explanation to the emission differences is the laser linewidths that when the Raman is stimulated with 532 nm, two lines are emitted from each

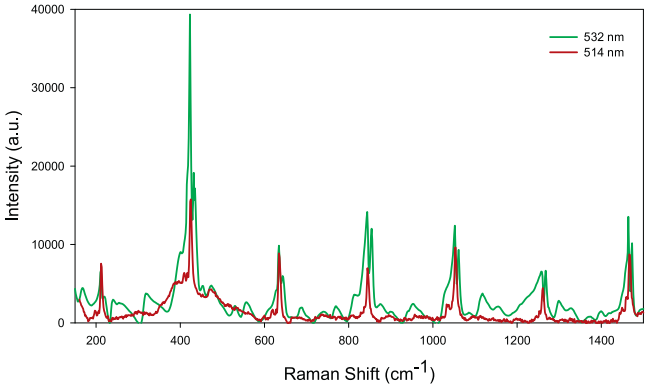

Fig. 4. SRS from the resonant vibrational mode when 532 nm (green plot) and 514.5 (brown plot) wavelengths are used for excitation.

shift while the narrower excitation of a gas laser generates only one emission line.

The spectrum obtained by a continuous excitation of the cubic phase with high laser power for about an hour is similar to that of $PbI_{2(s)}$ under high laser power excitation since after decomposition and evaporation of the formed gases, the main product of the crystal is $PbI_{2(s)}$ that undergoes further degradation [9,10]. Both spectra are presented in Figure S3.

4. Conclusions

In this work we present an investigation of several processes obtained from laser excitation of $MAPbI_3$ single crystal. The predicted process of phase transition from tetragonal to cubic phase was induced by excitation of over 15 mW laser power. The phases were characterized by LF-Raman and PL, taken simultaneously with the increase of exciting laser power and the spectral changes were assigned to the structural differences. In high laser power, the focused laser beam along with the sensitivity of the material, lead to decomposition only at the core of the focus. As a result, iodine vapors were trapped inside a cavity within the $MAPbI_3$ single crystal. Using wavelength excitation in the range of iodine absorption exhibited RRS of the spontaneous Raman signal which was stimulated. The SRS was enabled due to the $MAPbI_3$ unique properties, and even though this was a secondary process to the phase transition, the revealed properties can open a new frontier in investigating the $MAPbI_3$ for more applications. Future applications may include stimulation for Raman enhancement device or production of a tunable Raman laser based on iodine or any other RRS obtaining material.

Credit author statement

Tal Ben-Uliel & Hagit Aviv: Performed the measurements, studied literature, and wrote the paper.

Junjie Zhou: Crystallized $MAPbI_3$ single crystals.

Minghao Li: Suggested explanations for the results.

Shalom Avadyayev: Deposited $MAPbI_3$ thin films.

Omree Kapon & Vinayaka Damle: Worked on building optical set-up for this research.

Chenyi Yi & Yaakov Tischler: Supervised the work and reviewed the paper.

Declaration of Competing Interest

The authors declare no competing financial interest.

Acknowledgements

This work is supported by the National Natural Science Foundation of China (21872080), and Young Talents Thousand Program.

Appendix A. Supplementary data

Supplementary material related to this article can be found, in the online version, at doi:https://doi.org/10.1016/j.apmt.2020.100571.

References

[1] J.A. Turner, A realizable renewable energy future, Science 285 (1999) 687–689, http://dx.doi.org/10.1126/science.285.5428.687.
[2] T.T. Ava, A. Al Mamun, S. Marsillac, G. Namkoong, A review: thermal stability of methylammonium lead halide based perovskite solar cells, Appl. Sci. 9 (2019) 188–212, http://dx.doi.org/10.3390/app9010188.
[3] N. Espinosa, M. Hösel, D. Angmo, F.C. Krebs, Solar cells with one-day energy payback for the factories of the future, Energy Environ. Sci. 5 (2012) 5117–5132, http://dx.doi.org/10.1039/C1EE02728J.
[4] M.A. Green, A. Ho-Baillie, H.J. Snaith, The emergence of perovskite solar cells, Nat. Photonics 8 (2014) 506–514, http://dx.doi.org/10.1038/nphoton.2014.134.
[5] S. De Wolf, J. Holovsky, S.-J. Moon, P. Lö, B. Niesen, M. Ledinsky, F.J. Haug, J.H. Yum, C. Ballif, Organometallic halide perovskites: sharp optical absorption edge and its relation to photovoltaic performance, Phys. Chem. Lett. 5 (2014) 1035–1039, http://dx.doi.org/10.1021/jz500279b.
[6] L. Wang, G.D. Yuan, R.F. Duan, F. Huang, T.B. Wei, Z.Q. Liu, J.X. Wang, J.M. Li, Tunable bandgap in hybrid perovskite $CH_3NH_3Pb(Br_{3-y}X_y)$ single crystals and photodetector applications, AIP Adv. 6 (2016) 1–9, http://dx.doi.org/10.1063/1.4948312.
[7] A. Miyata, A. Mitioglu, P. Plochocka, O. Portugall, J. Tse-Wei Wang, S.D. Stranks, H.J. Snaith, R.J. Nicholas, Direct measurement of the exciton binding energy and effective masses for charge carriers in organic–inorganic tri-halide perovskites, Nat. Phys. 11 (2015) 582–588, http://dx.doi.org/10.1038/NPHYS3357.
[8] F. Zhang, B. Yang, Y. Li, W. Deng, R. He, Extra long electron-hole diffusion lengths in $CH_3NH_3PbI_{3-x}Cl_x$ perovskite single crystals, J. Mater. Chem. C 5 (2017) 8431–8435, http://dx.doi.org/10.1039/c7tc02802d.
[9] J.M. Frost, K.T. Butler, F. Brivio, C.H. Hendon, M. Van Schilfgaarde, A. Walsh, Atomistic origins of high-performance in hybrid halide perovskite solar cells terms of use, Nano Lett. 14 (2014), http://dx.doi.org/10.1021/nl500390f.
[10] E.J. Juarez-Perez, Z. Hawash, S.R. Raga, L.K. Ono, P.Y. Qi, Y. Qi, Thermal degradation of $CH_3NH_3PbI_3$ perovskite into NH_3 and CH_3I gases observed by coupled thermogravimetry–mass spectrometry analysis, Energy Environ. Sci. 9 (2016) 3406–3410, http://dx.doi.org/10.1039/c6ee02016j.
[11] F. Brivio, J.M. Frost, J.M. Skelton, A.J. Jackson, O.J. Weber, M.T. Weller, A.R. Goñi, A.M.A. Leguy, P.R.F. Barnes, A. Walsh, Lattice dynamics and vibrational spectra of the orthorhombic, tetragonal, and cubic phases of methylammonium lead iodide, Phys. Rev. B 92 (2015) 1–8, http://dx.doi.org/10.1103/PhysRevB.92.144308.
[12] X. Qian, X. Gu, R. Yang, Lattice thermal conductivity of organic-inorganic hybrid perovskite $CH_3NH_3PbI_3$, Appl. Phys. Lett. 108 (2016) 1–5, http://dx.doi.org/10.1063/1.4941921.
[13] X. Guo, C. McCleese, C. Kolodziej, A.C.S. Samia, Y. Zhao, C. Burda, Identification and characterization of the intermediate phase in hybrid organic–inorganic $MAPbI_3$ perovskite, Dalton Trans. 45 (2016) 3806–3813, http://dx.doi.org/10.1039/C5DT04420K.
[14] M.T. Weller, O.J. Weber, P.F. Henry, A.M. Di Pumpo, T.C. Hansen, Complete structure and cation orientation in the perovskite photovoltaic methylammonium lead iodide between 100 and 352 K, Chem. Commun. 51 (2015) 4180–4183, http://dx.doi.org/10.1039/C4CC09944C.
[15] B.J. Foley, D.L. Marlowe, K. Sun, W.A. Saidi, L. Scudiero, M.C. Gupta, J.J. Choi, Temperature dependent energy levels of methylammonium lead iodide perovskite, Appl. Phys. Lett. 106 (2015) 581–586, http://dx.doi.org/10.1063/1.4922804.
[16] Y. Liu, H. Lu, J. Niu, H. Zhang, S. Lou, C. Gao, Y. Zhan, X. Zhang, Q. Jin, L. Zheng, Temperature-dependent photoluminescence spectra and decay dynamics of $MAPbBr_3$ and $MAPbI_3$ thin films, AIP Adv. 8 (2018) 1–9, http://dx.doi.org/10.1063/1.5042489.
[17] C. Quarti, G. Grancini, E. Mosconi, P. Bruno, J.M. Ball, M.M. Lee, H.J. Snaith, A. Petrozza, F. De Angelis, The Raman spectrum of the $CH_3NH_3PbI_3$ hybrid perovskite: interplay of theory and experiment, J. Phys. Chem. Lett. 5 (2014) 279–284, http://dx.doi.org/10.1021/jz402589q.
[18] A.M.A. Leguy, A.R. Goñ, J.M. Frost, J. Skelton, F. Brivio, O.J.W. Xabier Rodrıǵuez-Martıńez, A. Pallipurath, M.I. Alonso, M. Campoy-Quiles, M.T. Weller, J. Nelson, A. Walshd, P.R.F. Barnes, Dynamic disorder, phonon lifetimes, and the assignment of modes to the vibrational spectra of methylammonium lead halide perovskites, Phys. Chem. Chem. Phys. 18 (2016) 27051–27066, http://dx.doi.org/10.1039/c6cp03474h.
[19] H.K. Hong, Theory of resonant Raman scattering. II. Overtones and hot bands, J. Chem, Phys. 67 (1977) 813–823, http://dx.doi.org/10.1063/1.434843.
[20] B. De Souza, G. Farias, F. Neese, R. Izsák, Efficient simulation of overtones and combination bands in resonant Raman spectra, J. Chem. Phys. 150 (2019) 1–9, http://dx.doi.org/10.1063/1.5099247.
[21] D.G. Fouche, R.K. Chang, Observation of resonance Raman scattering below the dissociation limit in I_2 vapor, Phys. Rev. Lett. 29 (1972) 536–539, http://dx.doi.org/10.1103/PhysRevLett.29.536.
[22] R.C. Prince, R.R. Frontiera, E.O. Potma, Stimulated Raman scattering: from bulk to nano, Chem. Rev. 117 (2017) 5070–5094, http://dx.doi.org/10.1021/acs.chemrev.6b00545.
[23] R.A. Bartels, S. Backus, M.M. Murnane, H.C. Kapteyn, Impulsive stimulated Raman scattering of molecular vibrations using nonlinear pulse shaping, Chem. Phys. Lett. 374 (2003) 326–333, http://dx.doi.org/10.1016/S0009-2614(03)00710-3.
[24] H. Pourbeyram, G.P. Agrawal, A. Mafi, Stimulated Raman scattering cascade spanning the wavelength range of 523 to 1750 nm using a graded-index multimode optical fiber, Appl. Phys. Lett. 102 (2013) 1–5, http://dx.doi.org/10.1063/1.4807620.
[25] X. Li, A.J. Lee, Y. Huo, H. Zhang, J. Wang, J.A. Piper, H.M. Pask, D.J. Spence, Managing SRS competition in a miniature visible $Nd:YVO_4/BaWO_4$ Raman laser, Opt. Express 20 (2012) 19305–19312, http://dx.doi.org/10.1364/oe.20.019305.
[26] Y.F. Chen, Compact efficient all-solid-state eye-safe laser with self-frequency Raman conversion in a $Nd:YVO_4$ crystal, Opt. Lett. 29 (2004) 2172–2174, http://dx.doi.org/10.1364/ol.29.002172.
[27] Y. Liu, F. Zhang, Z. Wang, F. Yu, L. Wei, X. Xu, X. Zhao, $Ca3(BO3)_2$, a first wide waveband borate Raman laser crystal with strong Raman effects and outstanding anti-optical damage ability, J. Mater. Chem. C 3 (2015) 10687–10694, http://dx.doi.org/10.1039/c5tc02067k.
[28] X. Wang, H. Qi, Y. Li, F. Yu, H. Wang, F. Chen, Y. Liu, Z. Wang, X. Xu, X. Zhao, Synthesis and characterization of new $Sr_3(BO_3)_2$ crystal for stimulated Raman scattering applications, Crystals 7 (2017) 1–9, http://dx.doi.org/10.3390/cryst7050125.
[29] E. Mosconi, C. Quarti, T. Ivanovska, G. Ruani, F. De Angelis, Structural and electronic properties of organo-halide lead perovskites: a combined IR-spectroscopy and ab initio molecular dynamics investigation, Phys. Chem. Chem. Phys. 16 (2014) 16137–16144, http://dx.doi.org/10.1039/c4cp00569d.
[30] C. Quarti, E. Mosconi, J.M. Ball, V. D'Innocenzo, C. Tao, S. Pathak, H.J. Snaith, A. Petrozza, F. De Angelis, Structural and optical properties of methylammonium lead iodide across the tetragonal to cubic phase transition: implications for perovskite solar cells, Energy Environ. Sci. 9 (2016) 155–163, http://dx.doi.org/10.1039/c5ee02925b.
[31] A.E. Williams, P.J. Holliman, M.J. Carnie, M.L. Davies, D.A. Worsley, T.M. Watson, Perovskite processing for photovoltaics: a spectro-thermal evaluation, J. Mater. Chem. A 2 (2014) 19338–19346, http://dx.doi.org/10.1039/c4ta04725g.
[32] G. Popov, M. Mattinen, T. Hatanpä, M. Vehkamä, M. Kemell, K. Mizohata, J. Rä Isä Nen, M. Ritala, M. Leskelä, Atomic layer deposition of PbI_2 thin films, Chem. Mater. 31 (2019) 1101–1109, http://dx.doi.org/10.1021/acs.chemmater.8b04969.
[33] T. Kiviniemi, J. Aumanen, P. Myllyperkiö, V.A. Apkarian, M. Pettersson, Time-resolved coherent anti-Stokes Raman-scattering measurements of I_2 in solid Kr: vibrational dephasing on the ground electronic state at 2.6–32 K, J. Chem. Phys. 123 (2005) 1–8, http://dx.doi.org/10.1063/1.1990115.
[34] W. Kiefer, H.J. Bernstein, Vibrational-rotational structure in the resonance Raman effect of iodine vapor, J. Mol. Spectrosc. 43 (1972) 366–381, http://dx.doi.org/10.1016/0022-2852(72)90048-3.
[35] J.C. Williamson, Teaching the rovibronic spectroscopy of molecular iodine, J. Chem. Educ. 84 (2007) 1355–1359, http://dx.doi.org/10.1021/ed084p1355.
[36] R. Zhang, J. Fan, X. Zhang, H. Yu, H. Zhang, Y. Mai, T. Xu, J. Wang, H.J. Snaith, Nonlinear optical response of organic–inorganic halide perovskites, ACS Photonics 3 (2016) 371–377, http://dx.doi.org/10.1021/acsphotonics.5b00563.
[37] J. Xu, X. Li, J. Xiong, C. Yuan, S. Semin, T. Rasing, X. Bu, Halide perovskites for nonlinear optics, Adv. Mater. (2019) 1806736, http://dx.doi.org/10.1002/adma.201806736.
[38] Y. Han, S. Meyer, Y. Dkhissi, K. Weber, J.M. Pringle, U. Bach, L. Spiccia, Y.B. Cheng, Degradation observations of encapsulated planar $CH_3NH_3PbI_3$ perovskite solar cells at high temperatures and humidity, J. Mater. Chem. A 3 (2015) 8139–8147, http://dx.doi.org/10.1039/C5TA00358J.
[39] J. Yang, B.D. Siempelkamp, D. Liu, T.L. Kelly, Investigation of $CH_3NH_3PbI_3$ degradation rates and mechanisms in controlled humidity environments using in situ techniques, ACS Nano 9 (2015) 1955–1963, http://dx.doi.org/10.1021/nn506864k.